NRC·CNRC

NRC Publications Archive
Archives des publications du CNRC

Electrochemical promotion of bimetallic palladium-cobalt nano-catalysts for complete methane oxidation

Ahledel, Najmeh; Saini, Komalpreet Kaur; Couillard, Martin; Baranova, Elena A.

This publication could be one of several versions: author's original, accepted manuscript or the publisher's version. / La version de cette publication peut être l'une des suivantes : la version prépublication de l'auteur, la version acceptée du manuscrit ou la version de l'éditeur.
For the publisher's version, please access the DOI link below./ Pour consulter la version de l'éditeur, utilisez le lien DOI ci-dessous.

Publisher's version / Version de l'éditeur:
https://doi.org/10.1002/cctc.202301363
ChemCatChem, 16, 5, 2024-01-08

NRC Publications Archive Record / Notice des Archives des publications du CNRC :
https://nrc-publications.canada.ca/eng/view/object/?id=53aa8fbd-eaa5-4066-9bbf-e992e8986134
https://publications-cnrc.canada.ca/fra/voir/objet/?id=53aa8fbd-eaa5-4066-9bbf-e992e8986134

Access and use of this website and the material on it are subject to the Terms and Conditions set forth at
https://nrc-publications.canada.ca/eng/copyright
READ THESE TERMS AND CONDITIONS CAREFULLY BEFORE USING THIS WEBSITE.

L'accès à ce site Web et l'utilisation de son contenu sont assujettis aux conditions présentées dans le site
https://publications-cnrc.canada.ca/fra/droits
LISEZ CES CONDITIONS ATTENTIVEMENT AVANT D'UTILISER CE SITE WEB.

Questions? Contact the NRC Publications Archive team at PublicationsArchive-ArchivesPublications@nrc-cnrc.gc.ca. If you wish to email the authors directly, please see the first page of the publication for their contact information.

Vous avez des questions? Nous pouvons vous aider. Pour communiquer directement avec un auteur, consultez la première page de la revue dans laquelle son article a été publié afin de trouver ses coordonnées. Si vous n'arrivez pas à les repérer, communiquez avec nous à PublicationsArchive-ArchivesPublications@nrc-cnrc.gc.ca.

National Research Council Canada | Conseil national de recherches Canada

Canada

Check for updates

ChemCatChem

Research Article
doi.org/10.1002/cctc.202301363

Chemistry Europe
European Chemical Societies Publishing

www.chemcatchem.org

Electrochemical Promotion of Bimetallic Palladium-Cobalt Nano-Catalysts for Complete Methane Oxidation

Najmeh Ahledel,[a] Komalpreet Kaur Saini,[a] Martin Couillard,[b] and Elena A. Baranova*[a]

The catalytic activity and electrochemical promotion of catalysis (EPOC) of the bimetallic Pd–Co nanoparticles (10 nm) deposited on yttria-stabilized zirconia were investigated for complete methane oxidation. The reaction was conducted under open-circuit and under polarization in a temperature range of 320–400 °C in reducing, stoichiometric, and oxidizing conditions. The catalytic activity of the catalyst nanoparticles increased to 40% upon positive polarization in all gaseous compositions. A comparison of three reaction conditions revealed that the highest reaction rate increase (enhancement ratio, $\rho = 1.4$) occurs under reducing conditions. The reaction rate increased upon anodic polarization, resulting in non-Faradaic electrochemical modification of catalytic activity ($\Lambda \gg 1$) in reducing and oxidizing conditions and Faradaic or electrochemical enhancement ($\Lambda < 1$) in stoichiometric reaction condition. This work demonstrates that the formation of different Pd and Co oxide phases can be accurately controlled by electrochemical stimuli and, in reducing conditions, result in pseudo-capacitor behaviour.

1. Introduction

Natural gas attracted attention due to its high energy density and low environmental impacts compared to other fossil fuels.[1] However, the lean-burn engines that consume natural gas often suffer from methane slip.[2] Considering that methane is a potent greenhouse gas, current regulations emphasize the need for more efficient, durable, and clean exhaust gas abatement systems for methane.[3,4] Typically, palladium catalysts are used in stationary and mobile exhaust gas abatement systems. However, these catalysts have several limitations associated with their stability and the activation of methane due to aging and sintering.[5] Furthermore, the high activity of methane oxidation has been shown to depend on the conversion of palladium into palladium oxide on the surface of the metallic Pd or the bulk palladium oxide. Since the exact composition of the palladium oxide is difficult to evaluate, the oxide is generally referred to as PdO_x instead of the stochiometric PdO. Adding a less expensive and more abundant non-noble metal to palladium catalyst is an effective way of modifying the surface properties of nanoparticles and consequently improving their catalytic performance.[6] The benefits of adding a second metal to create a bimetallic catalyst have been reported in heterogeneous catalysis.[7–9] In particular, transition metals with partially filled 3d orbital electrons and unique redox properties have attractive properties as a co-catalyst for Pd.[9] Some metals, such as Fe, Co, and Sn, can inhibit the sintering of the active PdO phase, while other metals, such as Ni and Zn, can increase the thermal stability of PdO compared to a monometallic Pd catalyst.

Cobalt and cobalt oxides are particularly promising catalysts for methane oxidation due to an electron donation effect that results in superior catalytic reactivity.[10] Furthermore, Co-based compounds (e.g., Co_3O_4, $Co(OH)_2$, CoOOH, and CoS) are some of the most well-known inorganic electrochemical capacitors. The charge storage mechanisms of these electrochemical capacitors are called pseudo capacitors (also known as redox and faradaic supercapacitors) and are based on reversible redox reactions at the surface of electrodes.[11] This surface redox reaction may affect the catalyst properties, in particular for oxidation reaction.

The phenomenon referred to as the electrochemical promotion of catalysis (EPOC) or the non-Faradaic electrochemical modification of catalytic activity (NEMCA) was first reported by Vayenas[12] in 1981. These concepts describe the change in the rates of catalytic reactions due to the application of an electric current or potential to the catalyst deposited on the solid electrolyte.[14–16] The migration of ions from the solid electrolyte to or from the surface of the catalyst results in remarkable changes in the catalytic activity and, in some cases, selectivity. The origin and fundamentals of this phenomenon are well documented and confirmed through many in-situ and ex-situ techniques,[14] as well as quantum-mechanical calculations.[18–23] The EPOC effect is also termed a non-Faradaic electrochemical modification of catalytic activity (NEMCA) due to the fact that the observed change in the reaction rate under polarization is much higher than the rate increase expected using Faraday's law.[13,15] This non-Faradaic enhancement is

[a] N. Ahledel, K. K. Saini, Prof. E. A. Baranova
Department of Chemical and Biological Engineering, Centre for Catalysis Research and Innovation (CCRI), Nexus for Quantum Technologies (NexQT)
University of Ottawa, 161 Louis-Pasteur, Ottawa ON, K1N 6N5
E-mail: elena.Baranova@uottawa.ca

[b] M. Couillard
National Research Council of Canada,
1200 Montreal Road, Ottawa, Ontario K1 A 0R6, Canada

Supporting information for this article is available on the WWW under https://doi.org/10.1002/cctc.202301363

© 2024 The Authors. ChemCatChem published by Wiley-VCH GmbH. This is an open access article under the terms of the Creative Commons Attribution Non-Commercial NoDerivs License, which permits use and distribution in any medium, provided the original work is properly cited, the use is non-commercial and no modifications or adaptations are made.

© 2024 The Authors. ChemCatChem published by Wiley-VCH GmbH

denoted by the apparent Faradaic efficiency, Λ, which can be calculated using Equation 1:

$$\Lambda = \frac{r - r_0}{I/nF} \quad (1)$$

where r_0 and r are the open-circuit and the promoted (or closed-circuit) rates, respectively. The other relevant EPOC parameter is the enhancement ratio, which is defined as the proportion of the promoted rate to the open-circuit catalytic rate:

$$\rho = \frac{r}{r_0} \quad (2)$$

The application of the EPOC effect to nanostructured catalysts has attracted significant practical interest in the last two decades.[22,24–29] The electrochemical promotion of the Pd catalyst layer for methane oxidation has been investigated.[29–34,38] Matei et al.[41,42] studied the influence of the pre-treatment and the addition of ethylene on the methane oxidation reaction. They aimed to ignite methane oxidation at lower temperatures to increase the open and closed-circuit catalytic performance of Pd film. Jimenez-Borja et al.[23] compared the performance of stand-alone Pd films and Pd supported on CeO_2 (Pd/CeO_2) at 600 °C. The Pd/CeO_2 catalyst exhibited catalytic activity that was 14 times higher than that of pure Pd due to the oxygen storage capacity of ceria as well as subsequent PdO formation. In the case of methane oxidation, the reaction rate increases upon anodic polarization due to more oxygen coverage on the catalyst, while negative polarization results in a decrease in the reaction rate or "poisoning".[43,44] In another work,[25] the effect of different catalyst preparation techniques on the catalytic activity of Pd/CeO_2 was investigated. In addition to CeO_2, Zagoraios et al.[41] recently used a nano-dispersed Pd catalyst supported on a porous Co_3O_4 commercial powder deposited on yttria-stabilized zirconia (YSZ) solid electrolyte. They observed higher catalytic activity and a faster electrochemical response in Pd/Co_3O_4 compared to unsupported Pd due to the size of the Pd nanoparticles as well as the presence of Co_3O_4, which acts as a "bridge" that allows $O^{\delta-}$ promoter ions to reach the metal nanoparticles.

Previous EPOC studies for methane oxidation (involving over 100 other catalytic systems) have been performed on continuous thin-film catalysts.[30] The electrochemical promotion of several noble and non-noble mono- and bi-metallic nanoparticles has been reported.[18,26,46–48] Recent work from our group demonstrated that nanostructured mono-metallic Pd and bi-metallic Ni_9Pd_1 nanoparticles can be efficiently electrochemically promoted.[25,49] They also reported that this behaviour persisted in the promoted catalyst and that this longer-lasting persistent promotion (p-EPOC) increased at longer polarization times.[34] The permanent EPOC effect was also reported in other studies due to the electrochemical oxidation or reduction of catalysts during the Pd–PdO transition.[32,38,40] Under oxidizing conditions, the permanent EPOC effect could be attributed to the electrochemical oxidation of metallic Pd in the presence of excess oxygen ions to PdO species, which is the active phase in methane oxidation reactions.[23]

Bimetallic nano-catalysts and their implementation in solid-state electrochemical cells for efficient polarization and promotion have been the subject of recent studies.[24,27,50,51] Hajar et al.[37] compared the performance of a Pd–Ni catalyst to a monometallic Pd catalyst at 425 °C and 500 °C. They found that Ni_9Pd exhibited a higher degree and more reversible electrochemical promotion compared to monometallic Pd nanoparticles when a positive current was applied. Therefore, in this study, we investigated bi-metallic Pd_8Co_2 to decrease the amount of expensive Pd, promote and stabilize Pd by adding Co and finally investigate EPOC effect. To attain those objectives, bimetallic Pd_8Co_{23} nanoparticles were synthesized using the polyol method and deposited on YSZ to investigate the influence of the EPOC effect on the activity of the catalyst for the complete methane oxidation reaction at low temperatures (320–400 °C) with various gas compositions. First, the detailed physicochemical characterization of Pd_8Co_2 was presented, then the catalytic performance of the catalyst and kinetics of the reaction under the open-circuit condition were reported. Lastly, the results of electrochemical studies using transient under positive and negative applied potential as well as cyclic voltammetry of Pd_8Co_2 nanoparticles are discussed.

2. Materials and Methods

2.1. Synthesis and Deposition of the Pd_8Co_2 Nanoparticle Catalyst

Bimetallic Pd_8Co_2 nanoparticles were prepared using a two-step polyol method.[38] The first step involves the production of Co nanoparticles by dissolving 0.437 g of cobalt (II) nitrate hexahydrate salt (Aldrich, 99.999%) in ethylene glycol, followed by the addition of 0.25 M tetra-methyl ammonium hydroxide pentahydrate (TMAOH; Sigma Aldrich, 97%) to increase the pH of the solution to 12. The cobalt solution was then refluxed at 160 °C for 2 hours. The second step involved the preparation of a separate solution of 133 mg of palladium chloride in 5 mL of ethylene glycol and 10μL of HCl (35.5–37%). This solution was then added to the cobalt solution, aiming to form Pd_8Co_2 nanoparticles with additional Pd particles on the surface. The mixture was refluxed for an additional 30 min to ensure the complete reduction of precursor salts, which could be monitored as the colour of the mixture turned black and the pH was reduced from 12 to 8. After the final solution was cooled to room temperature, it was washed with ethanol, centrifuged three times with additional ethanol washes in between, and dried at room temperature. The resulting Pd_8Co_2 nanoparticles were dispersed in isopropanol to make an ink with a concentration of 0.5 mg/mL. The Pd_8Co_2 catalyst was analyzed through the ICP-MS technique, and the measured atomic ratio of Pd to Co was 77 to 23 of Pd to Co. Therefore, the nanoparticles are denoted as Pd_8Co_2. Monometallic palladium

© 2024 The Authors. ChemCatChem published by Wiley-VCH GmbH

18673899, 2024, 5, Downloaded from https://chemistry-europe.onlinelibrary.wiley.com/doi/10.1002/cctc.202301363 by National Research Council, Wiley Online Library on [18/06/2024]. See the Terms and Conditions (https://onlinelibrary.wiley.com/terms-and-conditions) on Wiley Online Library for rules of use; OA articles are governed by the applicable Creative Commons License

18673899, 2024, 5, Downloaded from https://chemistry-europe.onlinelibrary.wiley.com/doi/10.1002/cctc.202301363 by National Research Council, Wiley Online Library on [18/06/2024]. See the Terms and Conditions (https://onlinelibrary.wiley.com/terms-and-conditions) on Wiley Online Library for rules of use; OA articles are governed by the applicable Creative Commons License

nanoparticles were prepared following the second step described above.

2.2. Physicochemical Techniques

The crystalline structure of Pd_8Co_2 and Pd NPs was examined by X-ray diffraction (XRD) using a Rigaku Ultima IV multipurpose diffractometer equipped with an X'Celerator detector for CuKα radiation. The scan was performed between 20 and 80 degree 2θ with a step of 0.03°/s.

The morphology of deposited catalysts was analyzed using scanning electron microscopy (SEM) using a PhenomTM scanning electron microscope (Nanoscience Instruments, Virginia, USA). The distribution of elements over the catalysts was studied using an FEI Titan^3 80–300 transmission electron microscopy (TEM) operated at 300 keV fitted with a CEOS aberration corrector and an Energy Dispersive X-ray spectrometer (EDAX Analyzer, DPP-II). A Gatan Tridiem 866 Image Filter performed electron energy loss spectroscopy (EELS) and energy-dispersive X-ray spectroscopy (EDX). High-angle annular dark-field (HAADF) imaging and energy dispersive X-ray spectroscopy (EDS) mapping were performed using the Fischione detector in a scanning transmission electron microscope (STEM). The STEM images and the EELS and EDX spectra were obtained according to the procedure described in.[39]

The XPS spectra were produced with the help of Kratos AXIS Nova spectrometer equipped with an Al X-ray source using AlK_α radiation at a 1486.69 eV charge neutralizer. The peak fits for high-resolution spectra are checked using the "Test Peak Model" program in CasaXPS software. The procedure used for fitting Co2p is described in.[40] The data were corrected for energy shifts due to the charging of the sample under the influence of the X-rays and corrected for the background using the Shirley (C1s) and Spline Shirley (Co2p, O1s, Pd3d) algorithms.

2.3. Electrochemical cell and reactor

The solid electrolytes were produced as 18 mm diameter and 2 mm thickness discs made of YSZ stabilized with 8 mol% Y_2O_3 as reported in more detail elsewhere.[41] On one side of the disc, the inert gold pseudo-reference (RE) and counter electrodes (CE) were painted using gold paste coating (TED PELLA Inc. USA), with the surface area of RE and CE being 0.2 and 1 cm^2, respectively, followed by a heating process in the air at 500 °C. The catalyst-working electrode (WE) was deposited on the solid electrolyte disc directly opposite the counter electrode (1 cm^2 surface area). Specifically, the catalyst nanoparticle ink was deposited using 10 μL at a time with subsequent heating at 60 °C for 2 min between deposits to dry the solution until the 1 mg loading of the Pd_8Co_2 catalyst was achieved. Lastly, a gold mesh was positioned on the working electrode side of the electrolyte to serve as a current collector, while the counter and reference electrodes were connected directly to the gold wires.[42] The electrical stimuli were applied and measured using the three gold wires connecting the electrodes to the potentiostat-galvanostat (Arbin Instruments, MSTAT). The temperature of the reactor was measured and controlled using two K-type thermocouples (OMEGA®). They were placed in the vicinity of the electrochemical cell inside the single-chamber capsule reactor.

Catalytic activity measurements were conducted at atmospheric pressure under continuous flow. The reactant gas mixture consisted of methane (Messr, 99.99%), oxygen (Linde, 99.90%), and a carrier gas of pure Argon (Messer, 99.99%). The gases were fed to the reactor through three independent mass flow controllers (OMEGA, 5500A Series) with a 100 mL/min flow rate. The produced CO_2 gas was analyzed using an infrared gas analyzer (Horiba, VA-3000). The whole reactor was housed within a tubular furnace connected to a temperature controller.

3. Results and Discussion

3.1. Physicochemical Properties

The XRD patterns of the as-prepared Pd_8Co_2 and Pd nanoparticles presented in Figure 1 show three characteristic peaks for both catalysts at approximately 40, 46, and 67 °2θ. This revealed that the Pd_8Co_2 nanoparticles have a face-centred cubic (fcc) structure identical to that of the Pd crystalline structure. The (111) reflection has the highest peak among the three representative peaks. It can also be observed that the (111) and (220) peaks of the Pd_8Co_2 catalyst were slightly shifted towards higher 2θ values compared to their respective Pd peaks, suggesting the formation of a palladium-cobalt alloy.[43] Since the atomic size of Pd and Co are similar, the shift in the peak position is not very significant. However, the crystallites of Pd_8Co_2 catalysts were slightly larger compared to the Pd catalyst. A summary of the characteristics of the XRD peaks and the calculated crystallite sizes of the two catalysts are presented in Table S1.

The crystallite size was calculated using the Debye-Scherrer equation.

$$D = \frac{0.9\ \nu_{Cu}}{\beta_{\frac{1}{2}}\ \cos\ \theta} \tag{3}$$

where ν_{Cu} is the X-ray wavelength, $\beta_{1/2}$ is the line broadening over the full width at half maximum (FWHM) in radians, and θ is the Bragg angle.

Figure 2 depicts the TEM images of the monometallic Pd catalyst (Figure 2a) and the Pd_8Co_2 catalyst (Figure 2b). The resulting Pd_8Co_2 and Pd nanoparticles are spherical in shape with an average particle size range of 5 and 10 nm, which were agglomerated under the electron beam.

The morphology of the freshly deposited (just prepared) and used (after reaction) Pd_8Co_2 catalysts on the YSZ disc as observed using SEM are presented in Figure 2c and Figure 2d, respectively. The freshly deposited catalyst has a porous structure with a high active surface area, and the structure of

© 2024 The Authors. ChemCatChem published by Wiley-VCH GmbH

Research Article
doi.org/10.1002/cctc.202301363
Chemistry Europe
European Chemical Societies Publishing

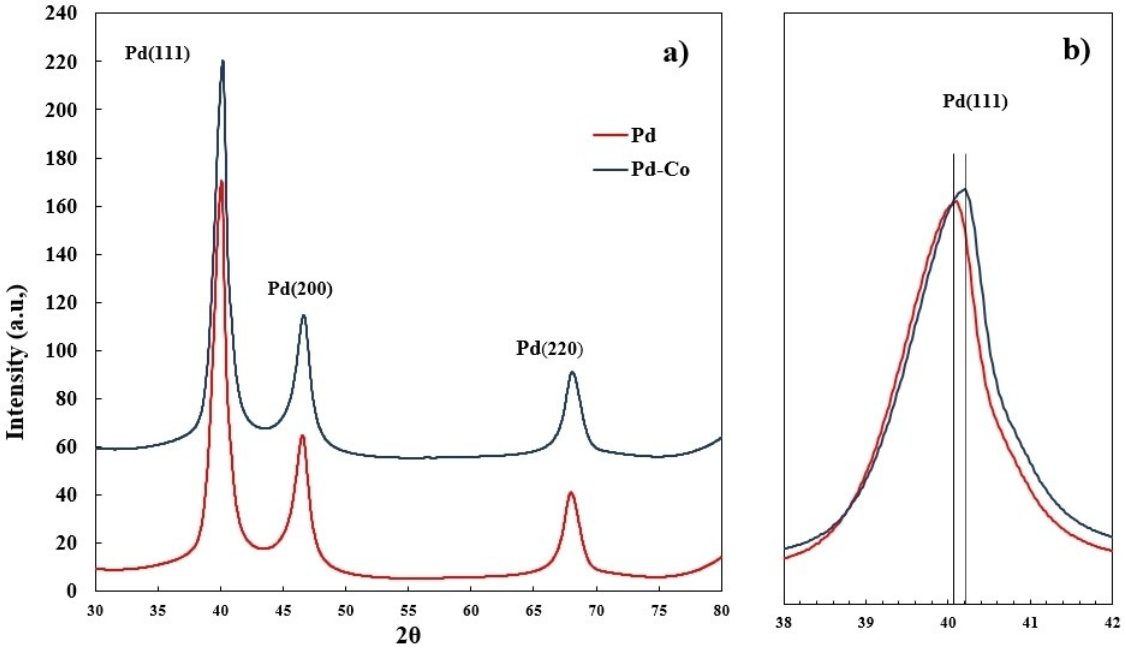

Figure 1. The XRD patterns of monometallic Pd (red) and bimetallic Pd_8Co_2(blue) nanoparticle catalyst (a) zoom to fcc (111) peak (b).

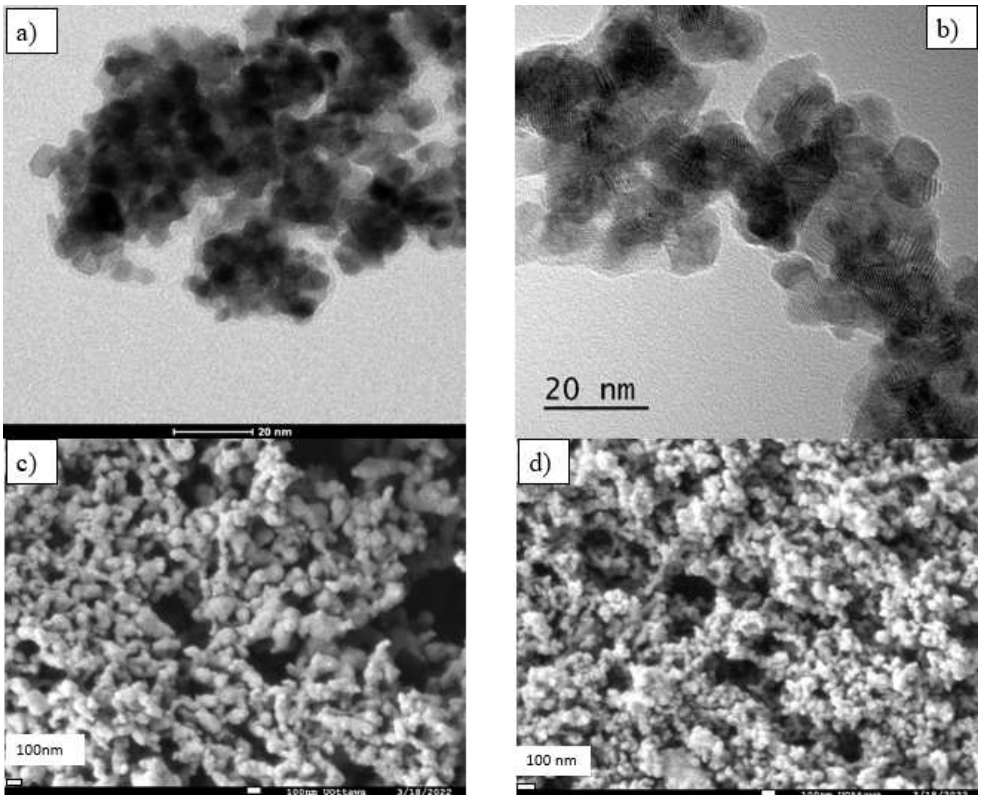

Figure 2. (a) TEM images of the Pd nanoparticles and (b) Pd_8Co_2 nanoparticles. SEM images of the Pd layer on the YSZ disc (c) before and (d) after electrochemical measurements.

the spent catalyst maintains its high porosity even after multiple tests and hours of experiments.

The structure and composition of the fresh Pd_8Co_2 catalyst were further investigated using ADF STEM-EDS and EELS. The morphology of the sample and its corresponding EELS

© 2024 The Authors. ChemCatChem published by Wiley-VCH GmbH

18673899, 2024, 5, Downloaded from https://chemistry-europe.onlinelibrary.wiley.com/doi/10.1002/cctc.202301363 by National Research Council, Wiley Online Library on [18/06/2024]. See the Terms and Conditions (https://onlinelibrary.wiley.com/terms-and-conditions) on Wiley Online Library for rules of use; OA articles are governed by the applicable Creative Commons License

elemental maps are presented in Figure S1. The overall composition of the catalyst is displayed in Figure S1a. The colours blue, green, and red represent the distribution of Co, O, and Pd, respectively, in Figure S1b-d as identified via EELS mapping and show that the distribution of both Pd and Co in the catalyst is nearly homogeneous. The presence of oxygen on the surface of the catalyst could indicate the formation of metal oxides during catalyst production. However, in some areas, the blue may represent the existence of a monometallic cobalt catalyst, which is associated with an amorphous structure, as confirmed by EDS analysis in area 3 in Figure S2.

The XPS spectra of the fresh sample are presented in Figure S3, which shows the surface composition of **the** catalyst. In particular, Figure S3a) shows the Pd2p region includes two sets of peaks attributed to metallic Pd and palladium oxide which indicates a mixture of Pd and PdO on the surface of the catalyst nanoparticles. In Figure S3b), the Co2p region peaks indicate the coexistence of two cobalt oxides, CoO and Co_3O_4. It should be noted that CoO could be oxidized to Co_3O_4 during XPS analysis. Table S2 summarizes the quantitative analysis of the XPS data associated with the Pd2p and the Co2p regions.

3.2. Catalytic oxidation of methane

The catalytic activity of the Pd_8Co_2 for complete methane oxidation reaction was investigated under open-circuit conditions under various gas compositions. Figure 3a shows the rate of CO_2 production as a function of temperature for different CH_4/O_2 ratios over the Pd_8Co_2 nanoparticles deposited on the YSZ disc. In all cases, the activation of the catalyst starts at 320 °C. More pronounced catalytic activity is observed at higher partial pressures of oxygen. Under oxidizing conditions ($CH_4/O_2 = 2:6$), the CO_2 formation rate at 400 °C was almost six times higher than under stoichiometric conditions ($CH_4/O_2 = 2:4$). The kinetics of the catalytic methane oxidation reaction was studied in steady-state mode by adjusting the partial pressures of oxygen and methane between 300–350 °C. The partial pressures of methane and oxygen varied between 0 and 20 kPa, while the partial pressure of the other reactant was kept at 2 kPa to determine the order dependence of the catalytic reaction rate. An increase in the partial pressure of methane (Figure 3c) led to an increase in the methane oxidation reaction rate. Thus, a positive-order dependence of the catalytic rate on methane was obtained, suggesting that methane is weakly bonded to the surface of the catalyst.

This rate law has been reported for methane oxidation over conventional Pd-based catalysts.[44] The effect of the partial pressure of oxygen on the catalytic rate is also presented in Figure 3b and has an insignificant influence on the reaction rate. Thus, the catalytic rate has a zero-order dependence with respect to the partial pressure of oxygen, highlighting the strong bonding of the oxygen on the surface of the catalyst, as shown in other studies.[45] The kinetic data suggest that the reaction exhibits a Langmuir-Hinshelwood mechanism based on the dissociative chemisorption of O_2.[22] In addition, there are rules relating the types of electrochemical responses of the

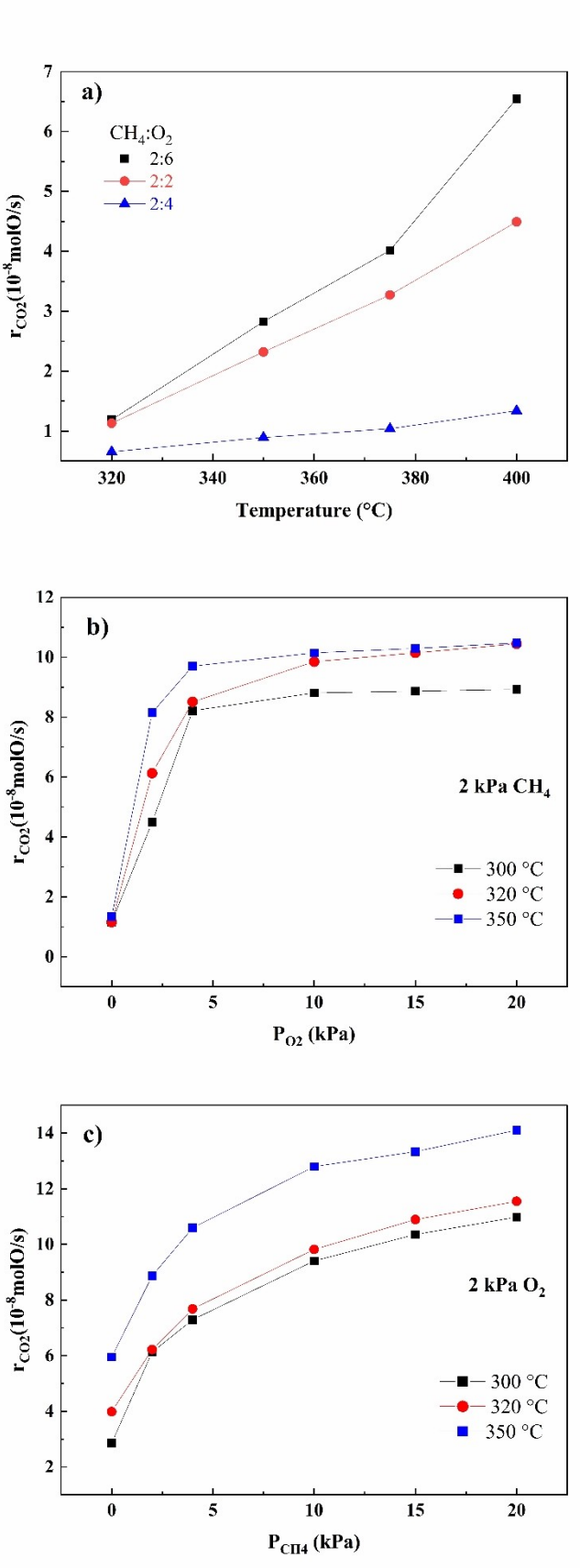

Figure 3. Methane oxidation rate under the open-circuit condition as a function of temperature (a) Partial pressure of CH_4 (b)and Partial pressure of O_2 (c).

© 2024 The Authors. ChemCatChem published by Wiley-VCH GmbH

18673899, 2024, 5, Downloaded from https://chemistry-europe.onlinelibrary.wiley.com/doi/10.1002/cctc.202301363 by National Research Council, Wiley Online Library on [18/06/2024]. See the Terms and Conditions (https://onlinelibrary.wiley.com/terms-and-conditions) on Wiley Online Library for rules of use; OA articles are governed by the applicable Creative Commons License

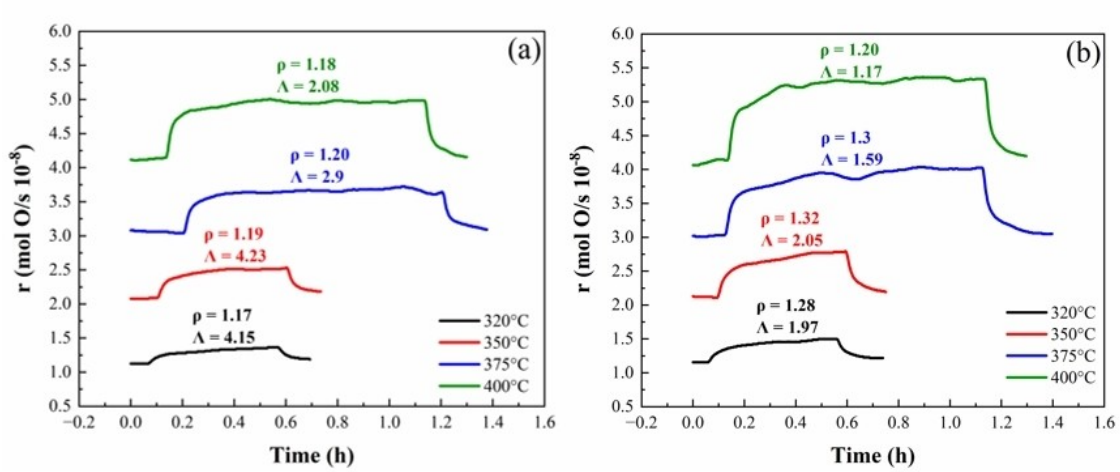

Figure 4. The transient effect of constant applied potentials of (a) +0.5 V and (b) + 1 V on the rate of CO2 formation in 2 kPa of CH4 and 2 kPa of O2 at different temperatures.

system to polarization and the kinetics of reactions under open-circuit conditions with respect to the electron acceptor and electron donor reactants.[13] In this case, based on the reaction order with respect to CH_4 as an electron donor and O_2 as an electron acceptor, the oxidation of methane over Pd_8Co_2 is expected to exhibit purely electrophobic behaviour, i.e., the rate enhancement under anodic polarization.

3.3. Electrochemical promotion of methane oxidation

Electrochemical evaluation experiments over Pd_8Co_2 nanoparticles were performed with several reactant gas compositions between 320 and 400 °C. Figure 4 shows a typical transient rate response and its corresponding current after the application of a constant positive potential (+0.5 V) between the Pd_8Co_2 catalyst-working electrode and the counter electrode at 350 °C under reducing conditions (CH_4:O_2 = 2:2). In its initial open-circuit state, the unpromoted catalytic rate, r_0, was found to be 2.1×10^{-8} mol O s^{-1}. The application of a constant potential resulted in a reaction rate increase. After 30 min of polarization, the reaction rate reached 2.5×10^{-8} mol O s^{-1}, a 20% increase compared to its open-circuit rate. The applied potential resulted in the migration of oxygen ions (O^{2-}) from the YSZ solid electrolyte to the Pd_8Co_2 catalyst electrode. The rate increase was four times greater than the back-spillover supply of O^{2-} – which had a rate of I/2F – indicating that each O^{2-} supplied to the surface of the catalyst allows four chemisorbed O atoms to react with methane. Therefore, the system exhibits non-Faradaic behaviour with a corresponding Faradaic efficiency of 4 and an enhancement rate of 1.2. After the interruption of polarization, the catalytic rate returns gradually and reversibly to its initial steady-state value.

Figure 5 presents the comparative transient responses of catalytic activity over the Pd_8Co_2 catalyst stoichiometric condition (CH_4:O_2 = :4) upon the application of a +0.5 V (Figure 5a) and a +1 V (Figure 5b) potential at different temperatures. The temperature had a positive effect on both the catalytic rate of the open circuit and the promoted reaction rate. The magnitude of the enhancement ratio (ρ) and the Faradaic efficiency (Λ) were found to peak at 350 °C because the solid electrolyte is less conductive at lower temperatures, while the effective double layer is less stable at elevated temperatures.

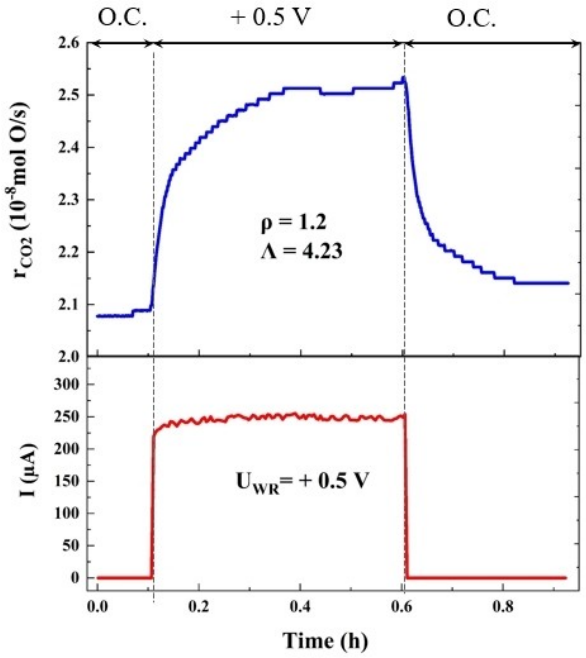

Figure 5. Transient response of the catalytic CO_2 formation rate and the produced current upon applying +0.5 V of potential at 350 °C under reducing conditions (CH_4:O_2 = 2:2).

Since the measured Λ values were greater than unity for all the examined reaction temperatures, it could be concluded that the catalytic activity enhancement is non-Faradaic, which is

© 2024 The Authors. ChemCatChem published by Wiley-VCH GmbH

18673899, 2024, 5, Downloaded from https://chemistry-europe.onlinelibrary.wiley.com/doi/10.1002/cctc.202301363 by National Research Council, Wiley Online Library on [18/06/2024]. See the Terms and Conditions (https://onlinelibrary.wiley.com/terms-and-conditions) on Wiley Online Library for rules of use; OA articles are governed by the applicable Creative Commons License

18673899, 2024, 5, Downloaded from https://chemistry-europe.onlinelibrary.wiley.com/doi/10.1002/cctc.202301363 by National Research Council, Wiley Online Library on [18/06/2024]. See the Terms and Conditions (https://onlinelibrary.wiley.com/terms-and-conditions) on Wiley Online Library for rules of use; OA articles are governed by the applicable Creative Commons License

evidence of the EPOC phenomenon. In addition, the reaction rate value returns to the open-circuit condition after polarization interruption, demonstrating reversible in-situ promotion of the catalyst.

Similar transient catalytic activity responses were observed (Figures S4, S5 and S6) in different reaction conditions after the application of positive potentials, which are summarized in Figure 6. The resulting reaction rate changes due to cathodic polarization are significantly less than those observed during anodic polarization, and no electrochemical promotion was observed. This behaviour is consistent with the electrophobic behaviour of the reaction (i.e., the catalytic rate increases with positive polarization). Since the methane oxidation reaction has a positive order with respect to CH_4 (the electron donor) and zero order with respect to O_2 (the electron acceptor) based on the kinetic results presented in section 3.2, electrophobic behaviour was expected according to the axioms of the EPOC effect. The observed electrophobic behaviour of the system can be attributed to the fact that, during electrochemical promotion, anodic polarization allows O^{2-} ions to migrate to the surface of the catalyst, strengthen chemisorbed oxygen as an electron-acceptor species, and weaken the binding strength of chemisorbed methane as an electron-donor species.[22] In addition, during electrochemical promotion, anodic polarization supplies the O^{2-} ions to the surface of the catalyst, leading to PdO formation at the three-phase boundary, which is an active phase for methane oxidation.[25,38] In stoichiometric conditions, the amount of Λ is less than unity, which means the rate increase is only due to the Faradaic reaction and phase transformation of Pd to PdO_x.

In the context of the partial pressure of oxygen in the gas mixture, the highest increase in catalytic rate was obtained under fuel-rich (oxidizing) conditions (Figure 6b), resulting in a ρ value of 1.44. The higher rates observed under this condition can be attributed to the lower oxygen coverage on the surface of the catalyst. In addition, at lower partial pressures of oxygen, the anodic polarization decreases the binding strength of oxygen on the catalyst surface. Consequently, more active adsorbed oxygen species are available to react with methane, which enhances the rate of oxidation.[49] Furthermore, under fuel-rich conditions, the desorption of oxygen is more likely due to the lower chemical potential of oxygen.

The catalyst exhibited a different electrochemical response at low partial pressures of oxygen (CH_4:O_2 = 2:1) compared to other gas mixture compositions. Figure 7 represents a typical transient response of the catalytic rate for the Pd_8Co_2 catalyst upon positive polarization of +1.5 V at 320 °C. It can be seen that the catalytic rate is constant under open-circuit conditions. Once polarization has commenced, CO_2 formation increases drastically and reaches a peak before decreasing and returning to its initial steady-state rate after 1.5 hours. Following the interruption of the applied potential, there was another sharp rate increase that exhibits the same behaviour as the previous peak. A similar electrochemical response was reported for Co and Fe-oxide catalysts in the reverse water gas shift reaction.[28]

In typical EPOC studies, the catalytic rate exhibits smooth and monotonic changes upon polarization and after potential interruption. Thus, two sharp peaks could be related to two processes:1) the electrochemical oxidation of the Pd_8Co_2 catalyst to a more active cobalt oxide catalyst for methane oxidation and 2) the formation of a pseudo-capacitor that can be charged and discharged upon polarization. An investigation of the corresponding change in current due to the application of the potential (Figure 7b) reveals a rapid increase in current immediately after the interruption of polarization, which could be indicating the discharging of the capacitor; this is likely to be what triggers the second peak in catalytic rate. Pseudo-capacitance reactions involve (quasi-) reversible reactions at the surface of electrodes.[11] Upon charging, ions (O^{2-}) are adsorbed onto an electrode; these ions are desorbed from the catalyst

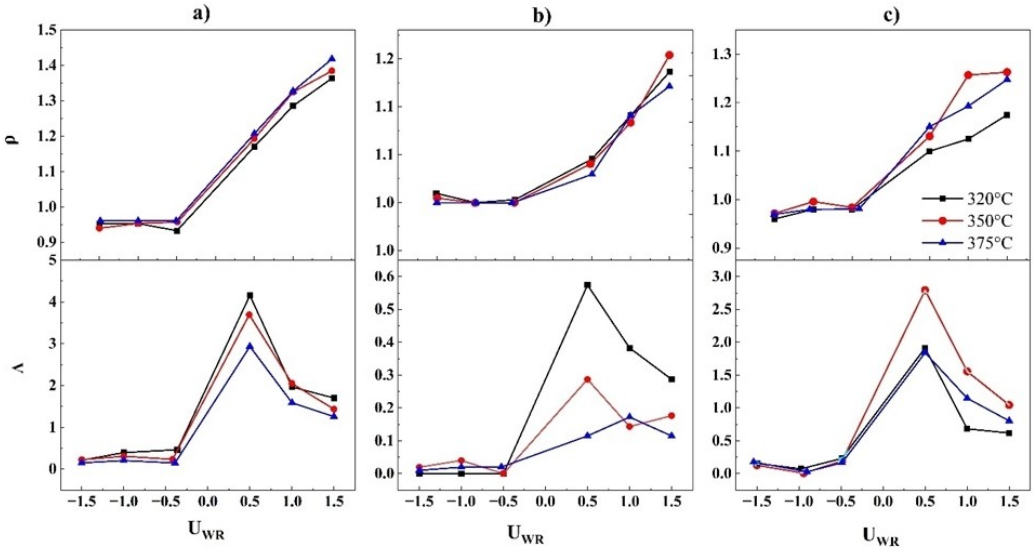

Figure 6. The effect of the applied potential on the maximum values of ρ and Λ under a) reducing reaction condition (CH_4:O_2 = 2:2), b) stoichiometric condition (CH_4:O_2 = 2:4), and c) oxidizing conditions (CH_4:O_2 = 2:6) at three different temperatures for the Pd_8Co_2 catalyst

© 2024 The Authors. ChemCatChem published by Wiley-VCH GmbH

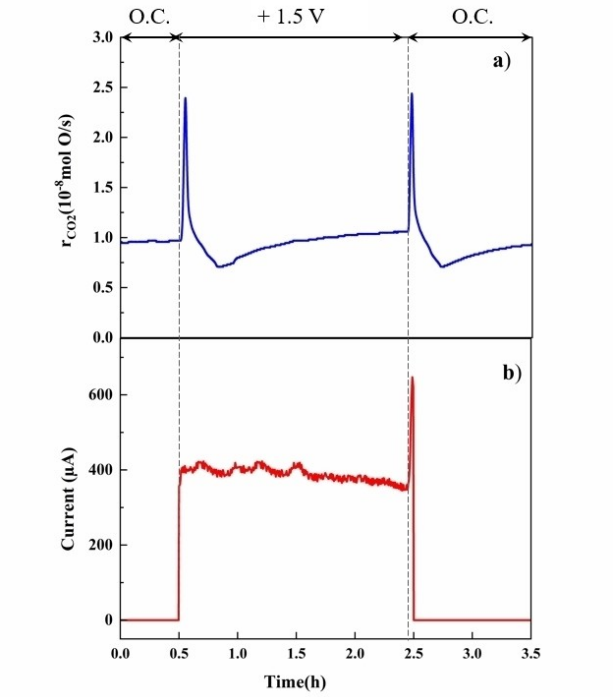

Figure 7. Transient effect of constant applied positive potential (+1.5 V) on the catalytic rate of methane oxidation and corresponding current in reducing condition ($CH_4:O_2=2:1$).

during discharge, with the electrons transferring through the external circuit. Pumping O^{2-} ions onto the surface could result in the phase transformation of cobalt oxide to a higher oxidation state while also being adsorbed onto the surface of the catalyst. The former may cause an increase in the catalytic rate since cobalt oxides have higher catalytic activity than cobalt,[51] while the latter generates the peak in current after the interruption of polarization, which functions as an instant in situ electrochemical polarization, resulting in a drastic catalytic rate increase.

Cobalt and cobalt oxides have been studied extensively for methane oxidation. The d orbitals of Co^{3+} and Co^{2+} in Co_3O_4 are unfilled, leading to relatively high C–H activation activity and, consequently, higher catalytic activity.[51] Zagoraios[35] reported the superior activity of nano-dispersed Pd supported on porous Co_3O_4 compared to pure Pd nanoparticles. Sun et al.[52] reported on the excellent catalytic properties of PdO-Co_3O_4 nanorods due to the synergistic relationship between PdO and Co_3O_4, which enhances the redox properties of the catalyst (i.e., easy oxidation and reduction), leading to greater methane activation capabilities at low temperatures.

Based on the above reports, it can be assumed that anodic polarization resulting from the pumping of O^{2-} promoters to the surface of the catalyst leads to an increase in the reaction rate (the first peak in Figure 7a) at the same time, it can charge the catalyst (due to its function as a pseudo-capacitor), which stores the charge during polarization and produces a current following the interruption of polarization (the second peak in Figure 7a). Similar peaks were reported during the polarization of Co nanoparticles in the reverse water gas shift reaction due to a change in oxidation state.[50] Thus, the lower activity that follows after the first peak observed during methane oxidation could be due to the oxidation of Co to less active cobalt oxides such as Co_2O_3 following Co_3O_4 formation during anodic polarization, which increases the work function of the catalyst during prolonged anodic polarization.

3.4. Electrochemical characterization of the Pd_8Co_2 catalyst

To investigate the change in the oxidation state of the Pd_8Co_2 catalyst, electrochemical measurements, including cyclic voltammetry (CV) and steady-state polarization curves, were carried out. The resulting CV is presented in Figure S7. The test was conducted under an inert atmosphere at 400°C between a range of potentials from −1.5 V to +1.5 V. Two peaks were observed during the anodic scan; these corresponded to the electrooxidation of Co by O^{2-} ions originating from the YSZ, followed by the evolution of oxygen at higher potentials. In the reverse scan, two cathodic peaks were observed, indicating the transition of cobalt oxide to two lower oxidation states.

The graphs in Figure 8a–c show the measured current as a function of the application of a potential between catalyst reference electrodes under reducing, stoichiometric, and oxidiz-

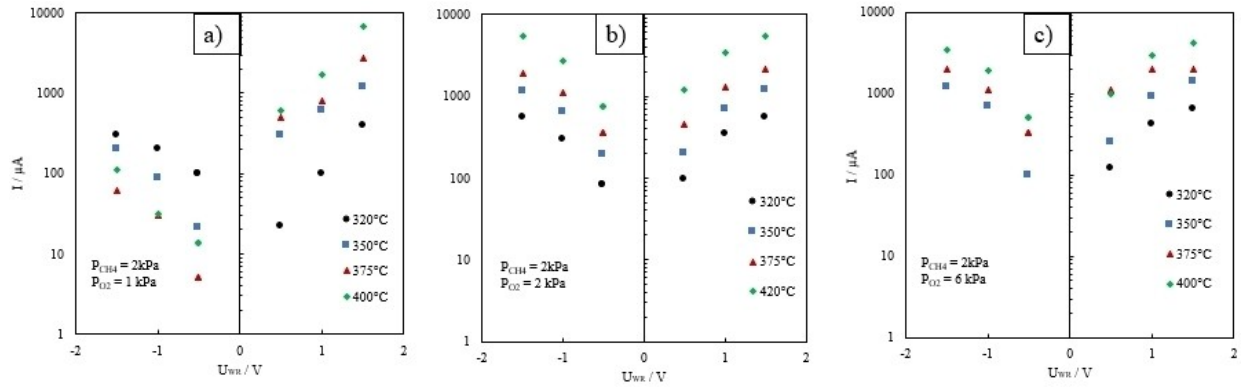

Figure 8. Polarization curve with the $CH_4:O_2$ gaseous ratio of (a)2:1, (b) 2:4, (c) 2:6, at four different temperatures.

© 2024 The Authors. ChemCatChem published by Wiley-VCH GmbH

18673899, 2024, 5, Downloaded from https://chemistry-europe.onlinelibrary.wiley.com/doi/10.1002/cctc.202301363 by National Research Council, Wiley Online Library on [18/06/2024]. See the Terms and Conditions (https://onlinelibrary.wiley.com/terms-and-conditions) on Wiley Online Library for rules of use; OA articles are governed by the applicable Creative Commons License

ing gaseous compositions at four different temperatures. The data points were collected from stable polarization conditions during the study of the EPOC effect.

The exchange current density was calculated by extrapolating the linear ln I vs. V (Tafel) section of the curves. Table S3. Summarizes the obtained values of i_o as calculated from the positive and negative branches, which shows an almost similar trend of changing exchange current density as a function of temperature for stoichiometric and oxidizing conditions (Figure 8 b, c), as was expected. In contrast, at lower partial oxygen pressures ($CH_4:O_2=2:1$), the shape of the two was found to be asymmetrical, suggesting that gaseous compositions with less oxygen promoted different electrochemical behaviours in the catalyst. In this case, the magnitude of the current at temperatures higher than 320 °C was smaller in the anodic region compared to the cathodic region, which may be due to the phase transition of the catalyst to lower oxidation states due to the application of negative polarization that is less likely in other reaction conditions in excess of oxygen ($CH_4:O_2=2:4$, $CH_4:O_2=2:6$ and $CH_4:O_2=2:2$).

Using the exchange current density (i_0) obtained from the electrochemical response of the catalysts at different temperatures and the following relationship, equation (4) was used to calculate the corresponding activation energy.

$$\ln\left(i_0\left(\mu A cm^{-2}\right)\right) = -\frac{E_a}{R}.\ 1/T + \ln A \quad (4)$$

E_a is the apparent activation energy (J/mol), R is the gas constant (8.314 J/mol K), T is the temperature (K), and A is the pre-exponential factor. The Arrhenius plots were produced for each reaction condition based on the cathodic and anodic branches of the Tafel plot, which are presented in Figure S8. The apparent activation energy has a negative value for the reducing condition, indicating a change in the electrochemical reaction compared to other reaction conditions.

Conclusions

This work aimed to study the electrochemical promotion of methane oxidation over Pd_8Co_2 nanoparticles deposited on a YSZ solid electrolyte under different gas compositions between 320–400 °C. Catalytic kinetic measurements predicted this reaction to exhibit electrophobic behaviour, which was consistent with the experimental results of the EPOC effect. The temperature and partial pressure of the reactant did not have a significant effect on the ρ and Λ values. However, the catalyst exhibited a different electrochemical response when the gaseous mixture had a low partial oxygen pressure (CH4:O2= 2:1) compared to other gas compositions similar to that of pseudo-capacitance reactions. Electrochemical characterization supported the behaviour observed under this gaseous composition. Our work demonstrates the importance of studies on electrochemical phenomena such as the EPOC effect as an in-situ tool that can provide insights into the oxidation state of the Pd_8Co_2 catalyst during methane oxidation as well as the potential of electrochemical capacitance formation. This study focused on the electrochemical enhancement of Pd_8Co_2 within the temperature range of 320–375 °C. This relatively low-temperature range is particularly favourable for methane oxidation, rendering the catalytic system potentially suitable for addressing methane slip issues in liquefied natural gas (LNG) engines, including those employed in marine transport or LNG vehicles. The rate increase could be improved at higher temperatures since the elevated temperature leads to higher conductivity of solid electrolytes and accelerates the O^{2-} migration.

Acknowledgements

The authors appreciate Dr. Yun Liu for her assistance with the SEM and TEM tests and Gabriele Schatte from Queen's University for her help with XPS. The authors thank the Natural Sciences and Engineering Research Council of Canada (NSERC) Discovery Grant (RGPIN05494), MITACS Accelerate Grant (IT16190) and BESANTEK Corporation for the financial support of this work.

Conflict of Interests

The authors declare no conflict of interest.

Data Availability Statement

The data that support the findings of this study are available from the corresponding author upon reasonable request.

Keywords: Electrochemical Promotion of the Catalysis (EPOC) · complete methane oxidation · yttria-stabilized zirconia (YSZ) · palladium-cobalt nanoparticles · oxidation · heterogeneous catalysis

[1] C. Lenox, P. O. Kaplan, *Energy Econ.* **2016**, *60*, 460–468.
[2] P. Lott, O. Deutschmann, *Emiss. Control Sci. Technol.* **2021**, *7*, 1–6.
[3] Z. Merrin, P. W. Francisco, *Environ. Sci. Technol.* **2019**, *53*, 5473–5482.
[4] H. Thomson, J. J. Corbett, J. J. Winebrake, *Energy Policy* **2015**, *87*, 153–167.
[5] T. R. Johns, J. R. Gaudet, E. J. Peterson, J. T. Miller, E. A. Stach, C. H. Kim, M. P. Balogh, A. K. Datye, *ChemCatChem* **2013**, *5*, 2636–2645.
[6] Piccolo, Laurent. "Surface studies of catalysis by metals: nanosize and alloying effects." In Nanoalloys: synthesis, structure and properties, pp. 369-404. London: Springer London, 2012.
[7] N. M. Martin, M. Van Den Bossche, A. Hellman, H. Grönbeck, C. Hakanoglu, J. Gustafson, S. Blomberg, N. Johansson, Z. Liu, S. Axnanda, J. F. Weaver, E. Lundgren, *ACS Catal.* **2014**, *4*, 3330–3334.
[8] W. Kumsung, M. Chareonpanich, P. Kongkachuichay, S. Senkan, A. Seubsai, *Catal. Commun.* **2018**, *110*, 83–87.
[9] H. Chauhan, S. Deka, *Fundam. Supercapacitor Appl. 2D Mater.* **2021**, 159–191.
[10] L. F. Liotta, H. Wu, G. Pantaleo, A. M. Venezia, *Catal. Sci. Technol.* **2013**, *3*, 3085–3102.
[11] K. K. Lee, W. S. Chin, C. H. Sow, *J. Mater. Chem. A* **2014**, *2*, 17212–17248.
[12] M. Stoukides, C. G. Vayenas, *J. Catal.* **1981**, *70*, 137–146.
[13] C. G. Vayenas, *Catal. Lett.* **2013**, *143*, 1085–1097.

© 2024 The Authors. ChemCatChem published by Wiley-VCH GmbH

18673899, 2024, 5, Downloaded from https://chemistry-europe.onlinelibrary.wiley.com/doi/10.1002/cctc.202301363 by National Research Council, Wiley Online Library on [18/06/2024]. See the Terms and Conditions (https://onlinelibrary.wiley.com/terms-and-conditions) on Wiley Online Library for rules of use; OA articles are governed by the applicable Creative Commons License

[14] B. D. Shepherd, R. West, *Chem. Lett.* **1988**, *17*, 183–186.
[15] S. Ladas, S. Bebelis, C. G. Vayenas, *Surf. Sci.* **1991**, *251–252*, 1062–1068.
[16] C. G. Vayenas, S. Bebelis, S. Neophytides, *J. Phys. Chem.* **1988**, *92*, 5083–5085.
[17] Vernoux, Philippe, and Constantinos G. Vayenas, eds. Recent advances in electrochemical promotion of catalysis. Springer, 2023.
[18] Y. M. Hajar, M. S. E. Houache, U. Tariq, P. Vernoux, E. A. Baranova, *ECS Trans.* **2017**, *77*, 51–66.
[19] P. Tsiakaras, C. G. Vayenas, *J. Catal.* **1993**, *140*, 53–70.
[20] C. Jiménez-Borja, F. Matei, F. Dorado, J. L. Valverde, *Appl. Surf. Sci.* **2012**, *261*, 671–678.
[21] C. Jiménez-Borja, F. Dorado, A. De, J. M. G. -Vargas, J. L. Valverde, *Fuel Cells* **2011**, pp. 131–139.
[22] C. Jiménez-Borja, B. Delgado, F. Dorado, J. L. Valverde, *Chem. Eng. J.* **2013**, *225*, 315–322.
[23] C. Jiménez-Borja, F. Dorado, A. de Lucas-Consuegra, J. M. García-Vargas, J. L. Valverde, *Catal. Today* **2009**, *146*, 326–329.
[24] Jiménez-Borja, C., F. Dorado, A. de L.-Consuegra, J. M. G.-Vargas, and J. L. Valverde. "Electrochemical promotion of CH4 combustion over a Pd/CeO2–YSZ catalyst." Fuel Cells 11, no. 1 (2011): 131-139.
[25] C. Jiménez-Borja, S. Brosda, F. Matei, M. Makri, B. Delgado, F. Sapountzi, D. Ciuparu, F. Dorado, J. L. Valverde, C. G. Vayenas, *Appl. Catal. B* **2012**, *128*, 48–54.
[26] Matei, F., D. Ciuparu, C. Jiménez-Borja, F. Dorado, J. L. Valverde, and S. Brosda. "Electrochemical promotion of methane oxidation on impregnated and sputtered Pd catalyst-electrodes deposited on YSZ." Applied Catalysis B: Environmental 127 (2012): 18-27.
[27] Jiménez-Borja, C., S. Brosda, M. Makri, F. Sapountzi, F. Dorado, J. L. Valverde, and C. G. Vayenas. "Methane oxidation on Pd/YSZ by electrochemical promotion." Solid State Ionics 225 (2012): 376-381.
[28] V. Roche, R. Revel, P. Vernoux, *Catal. Commun.* **2010**, *11*, 1076–1080.
[29] A. Nakos, S. Souentie, A. Katsaounis, *Appl. Catal. B* **2010**, *101*, 31–37.
[30] Vayenas, Costas G., Symeon Bebelis, Costas Pliangos, Susanne Brosda, and Demetrios Tsiplakides. Electrochemical activation of catalysis: promotion, electrochemical promotion, and metal-support interactions. New York: Kluwer Academic/Plenum Publishers, 2001.10.1007/B115566.
[31] Y. M. Hajar, L. Treps, C. Michel, E. A. Baranova, S. N. Steinmann, *Catal. Sci. Technol.* **2019**, *9*, 5915–5926.
[32] H. A. E. Dole, R. J. Isaifan, F. M. Sapountzi, L. Lizarraga, D. Aubert, A. Princivalle, P. Vernoux, E. A. Baranova, *Catal. Lett.* **2013**, *143*, 996–1002.
[33] C. Xia, M. Hugentobler, Y. Li, G. Foti, C. Comninellis, W. Harbich, *Electrochem. Commun.* **2011**, *13*, 99–101.
[34] Y. M. Hajar, B. Venkatesh, E. A. Baranova, *Catalysts* **2019**, *9*, 48.
[35] D. Zagoraios, A. Athanasiadi, I. Kalaitzidou, S. Ntais, A. Katsaounis, A. Caravaca, P. Vernoux, C. G. Vayenas, *Catal. Today* **2019**, DOI 10.1016/j.cattod.2019.02.030.
[36] V. Roche, R. Karoum, A. Billard, R. Revel, P. Vernoux, *J. Appl. Electrochem.* **2008**, *38*, 1111–1119.
[37] Hajar, Yasmine M., Balaji Venkatesh, Mohamed SE Houache, Hanshuo Liu, Reza Safari, Sagar Prabhudev, Gianluigi A. Botton, and Elena A. Baranova. "Electrochemical promotion of Bi-metallic Ni9Pd core double-shell nanoparticles for complete methane oxidation." Journal of Catalysis 374 (2019): 127-135..
[38] H. Dong, Y. C. Chen, C. Feldmann, *Green Chem.* **2015**, *17*, 4107–4132.
[39] C. Panaritis, J. Zgheib, S. A. H. Ebrahim, M. Couillard, E. A. Baranova, *Appl. Catal. B* **2020**, *269*, 118826.
[40] B. Vincent Crist, *Handb. Elem. Nativ. Oxides* **1999**, *1*, 1–87.
[41] H. Guo, T. J. M. Bayer, J. Guo, A. Baker, C. A. Randall, *J. Eur. Ceram. Soc.* **2017**, *37*, 2303–2308.
[42] H. A. E. Dole, A. C. G. S. A. Costa, M. Couillard, E. A. Baranova, *J. Catal.* **2016**, *333*, 40–50.
[43] L. Zhang, K. Lee, J. Zhang, *Electrochim. Acta* **2007**, *52*, 3088–3094.
[44] D. Ciuparu, M. R. Lyubovsky, E. Altman, L. D. Pfefferle, A. Datye, *Catal. Rev. Sci. Eng.* **2002**, *44*, 593–649.
[45] D. Ciuparu, E. Altman, L. Pfefferle, *J. Catal.* **2001**, *203*, 64–74.
[46] Panaritis, Christopher, Johnny Zgheib, Martin Couillard, and Elena A. Baranova. "The role of Ru clusters in Fe carbide suppression for the reverse water gas shift reaction over electropromoted Ru/FeOx catalysts." Electrochemistry Communications 119 (2020): 106824..
[47] S. Brosda, C. G. Vayenas, J. Wei, *Appl. Catal. B* **2006**, *68*, 109–124.
[48] C. Falgairette, A. Jaccoud, G. Fóti, C. Comninellis, *J. Appl. Electrochem.* **2008**, *38*, 1075–1082.
[49] A. D. Frantzis, S. Bebelis, C. G. Vayenas, *Electrochemical Promotion (NEMCA) of CH and C H Oxidation 4 2 4 on Pd/YSZ and Investigation of the Origin of NEMCA via AC Impedance Spectroscopy*, **2000**.
[50] D. Zagoraios, S. Tsatsos, S. Kennou, C. G. Vayenas, G. Kyriakou, A. Katsaounis, *ACS Catal.* **2020**, 14916–14927.
[51] L. F. Liotta, H. Wu, G. Pantaleo, A. M. Venezia, *Catal. Sci. Technol.* **2013**, *3*, 3085.
[52] Sun, Yongnan, Jingwei Liu, Nating Yang, and Yan Zhu. "One-Dimensional Heterostructured Palladium Oxide-Cobalt Oxide Catalyst for the Catalytic Oxidation of Methane." ChemCatChem 9, no. 5 (2017): 738-745.

Manuscript received: October 26, 2023
Revised manuscript received: January 4, 2024
Accepted manuscript online: January 8, 2024
Version of record online: February 12, 2024

© 2024 The Authors. ChemCatChem published by Wiley-VCH GmbH

18673899, 2024, 5, Downloaded from https://chemistry-europe.onlinelibrary.wiley.com/doi/10.1002/cctc.202301363 by National Research Council, Wiley Online Library on [18/06/2024]. See the Terms and Conditions (https://onlinelibrary.wiley.com/terms-and-conditions) on Wiley Online Library for rules of use; OA articles are governed by the applicable Creative Commons License